JACS
JOURNAL OF THE AMERICAN CHEMICAL SOCIETY

Subscriber access provided by ISTANBUL TEKNIK UNIV

Article

Nonadiabatic Deactivation of 9*H*-Adenine: A Comprehensive Picture Based on Mixed Quantum#Classical Dynamics

Mario Barbatti, and Hans Lischka

J. Am. Chem. Soc., **2008**, 130 (21), 6831-6839 • DOI: 10.1021/ja800589p • Publication Date (Web): 30 April 2008

Downloaded from http://pubs.acs.org on February 8, 2009

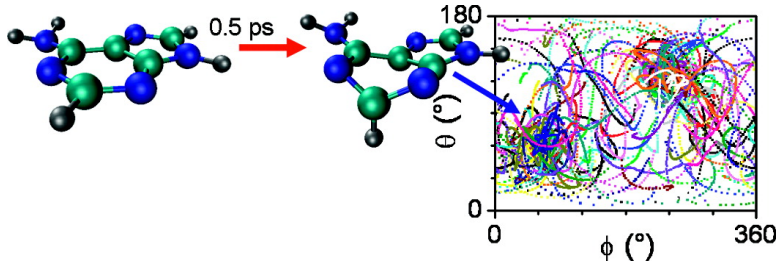

More About This Article

Additional resources and features associated with this article are available within the HTML version:

- Supporting Information
- Links to the 4 articles that cite this article, as of the time of this article download
- Access to high resolution figures
- Links to articles and content related to this article
- Copyright permission to reproduce figures and/or text from this article

View the Full Text HTML

ACS Publications
High quality. High impact.

Journal of the American Chemical Society is published by the American Chemical Society. 1155 Sixteenth Street N.W., Washington, DC 20036

J|A|C|S
ARTICLES

Published on Web 04/30/2008

Nonadiabatic Deactivation of 9*H*-Adenine: A Comprehensive Picture Based on Mixed Quantum−Classical Dynamics

Mario Barbatti* and Hans Lischka*

Institute for Theoretical Chemistry, University of Vienna, Waehringerstrasse 17, 1090-Vienna, Austria

Received January 24, 2008; E-mail: mario.barbatti@univie.ac.at; hans.lischka@univie.ac.at

Abstract: Mixed quantum−classical dynamics simulations at the multireference configuration interaction (MR-CIS) level were performed for 9*H*-adenine in order to understand its ultrafast nonradiative decay process. Dynamics simulations were also performed for the model system 6-aminopyrimidine. MR-CIS and complete active space perturbation theory (CASPT2) have been employed to characterize a large variety of qualitatively different conical intersections, the branches of the crossing seam connecting them, and the reaction paths from the Franck−Condon region for 9*H*-adenine. The results show a two-step process consisting of ultrashort deactivation from S_3 to S_1 and a longer exponential decay step corresponding to the conversion from S_1 to S_0.

Introduction

Femtosecond spectroscopy has shown that 9*H*-adenine (9*H*-Ade) returns in the gas phase to the ground state within approximately 1 ps after photoexcitation.[1–7] This ultrafast decay feature, also shared by the other nucleobases composing DNA and RNA, is believed to enhance the photostability of these molecules toward UV irradiation.[8] The experiments, however, have only indirectly provided structural information on the processes taking place during the deactivation. For this reason, besides the fact of ultrafast deactivation itself, there is no agreement about the mechanistic details of the processes, and the transient spectra for 9*H*-Ade and its derivatives have been analyzed in terms of one,[1] two,[4–6] and three[3] decay components.

From a theoretical point of view the situation is not better. In general, theoreticians have assumed that the decay proceeds through at least two steps, an ultrashort one taking place in about 100 fs and one or two longer steps proceeding in about 1 ps or more.[9–15] The most frequent interpretation says that the short step corresponds to the relaxation from the L_a-$\pi\pi^*$ state into the minimum of the S_1 state, while the long steps correspond to the time for the nonadiabatic deactivation at one of the S_1/S_0 conical intersections.[4,9,10,13,14] Part of the theoretical effort has been spent in assigning which conical intersection is predominant for each step on the basis of reaction paths.[9,10,14] The lowest energy conical intersection, which shows an envelope puckering at the C_2 atom (^{2}E conformation, see Figure 1 for numbering and Computational Details for notation), has been associated to the (long) 1 ps step and to the nonadiabatic transitions taking place after low-energy photoexcitation. The conical intersections showing a screw-boat conformation puckered at N_1 and C_6 atoms ($^1S_6$) have been associated with longer processes in time and high-energy excitations.[10,16] Those resulting from N−H stretching or C_8−N_9 bond breaking[14,17–19] have also been associated with high-energy excitations, although there is still not consensus about the threshold to activate these channels.[18,19]

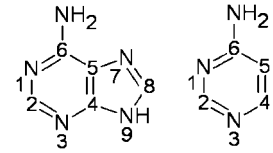

Figure 1. Geometry and numbering of 9*H*-adenine (9*H*-Ade) and 6-aminopyrimidine (6AP).

Recently, two rather different hypotheses have been raised to explain the short and long time step components.[5,6,15,20] On the basis of calculations of reaction paths at CASPT2 level, Serrano-Andrés and co-workers[15,20] proposed that the short step corresponds to a fast deactivation of a fraction of the 9*H*-Ade population passing through the S_1/S_0 ^{2}E conical intersection.

(1) Kang, H.; Lee, K. T.; Jung, B.; Ko, Y. J.; Kim, S. K. *J. Am. Chem. Soc.* **2002**, *124*, 12958–12959.
(2) Kang, H.; Jung, B.; Kim, S. K. *J. Chem. Phys.* **2003**, *118*, 6717–6719.
(3) Ullrich, S.; Schultz, T.; Zgierski, M. Z.; Stolow, A. *J. Am. Chem. Soc.* **2004**, *126*, 2262–2263.
(4) Canuel, C.; Mons, M.; Piuzzi, F.; Tardivel, B.; Dimicoli, I.; Elhanine, M. *J. Chem. Phys.* **2005**, *122*, 074316.
(5) Satzger, H.; Townsend, D.; Stolow, A. *Chem. Phys. Lett.* **2006**, *430*, 144–148.
(6) Satzger, H.; Townsend, D.; Zgierski, M. Z.; Patchkovskii, S.; Ullrich, S.; Stolow, A. *Proc. Natl. Acad. Sci. U.S.A.* **2006**, *103*, 10196–10201.
(7) Chin, C. H.; Mebel, A. M.; Kim, G. S.; Baek, K. Y.; Hayashi, M.; Liang, K. K.; Lin, S. H. *Chem. Phys. Lett.* **2007**, *445*, 361–369.
(8) Crespo-Hernández, C. E.; Cohen, B.; Hare, P. M.; Kohler, B. *Chem. Rev.* **2004**, *104*, 1977–2019.
(9) Blancafort, L.; Cohen, B.; Hare, P. M.; Kohler, B.; Robb, M. A. *J. Phys. Chem. A* **2005**, *109*, 4431–4436.
(10) Chen, H.; Li, S. H. *J. Phys. Chem. A* **2005**, *109*, 8443–8446.
(11) Marian, C. M. *J. Chem. Phys.* **2005**, *122*, 104314.
(12) Nielsen, S. B.; Solling, T. I. *ChemPhysChem* **2005**, *6*, 1276–1281.
(13) Perun, S.; Sobolewski, A. L.; Domcke, W. *J. Am. Chem. Soc.* **2005**, *127*, 6257–6265.
(14) Perun, S.; Sobolewski, A. L.; Domcke, W. *Chem. Phys.* **2005**, *313*, 107–112.
(15) Serrano-Andrés, L.; Merchán, M.; Borin, A. C. *Proc. Natl. Acad. Sci. U.S.A.* **2006**, *103*, 8691–8696.
(16) Blancafort, L. *J. Am. Chem. Soc.* **2006**, *128*, 210–219.

 © 2008 American Chemical Society

This conical intersection is found to be barrierlessly and diabatically connected to the Franck−Condon (FC) region, which would explain its extreme efficiency. The second and long step, still according to these authors, could be explained by the deactivation of the remaining part of the population via the $^1S_6$ conical intersection. On the other hand, on the basis of time-resolved photoelectron spectroscopy (TRPES) of 9*H*-adenine and 9-methyladenine, Satzger and co-workers[5,6] claim that for the 267 nm excitation the short step corresponds to the population of the $\pi\sigma^*$ state and the long step to decay into the S_0 state through the N_9-H stretching conical intersection. At lower wavelengths, however, the importance of this path would decrease, given the availability of other channels.

Because of its importance for biology, the photodynamics of adenine and its derivatives in the gas phase and in solution has been extensively investigated[8] with a large variety of experimental methods, starting from the early absorption spectra[21,22] to recent techniques such as laser double resonance (R2PI, UV−UV, IV−UV),[23–26] photoelectron (TRPES),[5,6] kinetic energy release (TKER),[3,19] and pump−probe transient[1–7] spectra. Concerning theoretical investigations, a large number of quantum-chemical methods, including CIS,[27] TD-DFT,[12,17] CC2,[28] DFT/MRCI,[11] CASPT2,[10,13–16,29] and MRCI,[18,30] have been employed in order to characterize the spectra,[28,29] cuts through the potential energy surfaces,[10,15] conical intersections,[11,13] and nonradiative decay rates.[7] To the best of our knowledge, despite this great variety of investigations, excited-state dynamics simulations have never been performed for adenine and this is the first report of this kind of investigation so far. Due to the size of the molecule, to the relatively long simulation times, and to the complexity of the electronic spectrum involving at least four electronic states, the performance of dynamics simulations is a formidable challenge. We have approached these challenges in several ways. First, we have performed dynamics calculations for 9*H*-Ade with the intention of investigating questions related to mechanisms taking place in about $^1/_2$ ps. Second, because of the numerical expense of these simulations, we decided to continue for longer time scales until 2 ps with a smaller adenine model, 6-aminopyrimidine (6AP) (see Figure 1), which has been proposed by us previously.[31] Third, the dynamics investigations are correlated with a comprehensive and systematic investigation of the seam of conical intersections and the reaction paths connecting the minima on the crossing seam to the Franck−Condon region of 9*H*-Ade. We shall demonstrate that this 3-fold strategy helps to understand the underlying mechanisms in the nonadiabatic deactivation and, in particular, to address the following issues raised by previous investigations. (i) Is the relaxation to the first excited singlet state responsible for the 100 fs short component? (ii) Can the ^2E conical intersection be activated on the 100 fs time scale as proposed by Serrano-Andrés et al.[15] or is it activated only at later times, in the picosecond range as discussed in the literature?[9–12,14] (iii) Is the $^1S_6$ conical intersection activated in the first few picoseconds of dynamics as proposed by several theoreticians?[9,10,14,15]

Computational Details

Stationary points and minima on the crossing seam (MXSs) were initially optimized at the complete active space self-consistent field level, including 12 electrons in 10 orbitals consisting of 9 π and 1 lone-pair (n) orbital (CASSCF(12,10)). Three states were included in the state averaging procedure (SA-3). The results were reoptimized at the multireference configuration interaction level, including single excitations from a reference space composed by six electrons in five orbitals (MR-CIS(6,5)), using the molecular orbitals obtained at the CASSCF(12,10) level. The MR-CIS reference space was constructed from the CASSCF(12,10) space by moving all orbitals with natural occupation larger than 0.9 for all stationary points and MXSs to the doubly occupied space and smaller than 0.1 to the virtual space. This approach was chosen since it improved significantly the accuracy of the CASSCF results, e.g. in terms of the ordering of vertical excitations, and was computationally still efficient enough to allow on-the-fly dynamics simulations. Single-point calculations for all optimized geometries (CASSCF and MR-CIS) were performed at the complete active space second-order perturbation theory level using 16 electrons, 12 orbitals (10 π and 2 n orbitals) and five states in the state averaging procedure (CASPT2/CASSCF(16,12)). Although no level shift was necessary, an IPEA shift of 0.25 was included.[32] This shift should correct the typical underestimation of the vertical excitation energies observed in the noncorrected zero-order Hamiltonian of the CASPT2 method. The 6-31G* basis set was used in all calculations unless stated otherwise.

Since conical intersections in heteroaromatic systems usually appear at several different puckered conformations, it is useful to provide a systematic characterization of them. This can be achieved by means of the Cremer−Pople (CP) parameters.[33] The ring puckering in an *N*-membered ring can be described by $N - 3$ parameters. In a spherical notation they are termed Q, θ and φ for six-membered rings and Q and φ for five-membered rings. The parameter Q describes the extent of the puckering. The other two parameters allow transformations between puckered rings.[34] For example, if we start with a six-membered ring with an envelope conformation, changing θ and keeping φ fixed will bring the ring into a boat conformation. The $\theta-\varphi$ space is particularly useful for mapping the crossing seam in six-membered-ring systems. The CP parameters[33] were computed according to the numbering scheme shown in Figure 1. The conformations of the six-membered puckered rings were determined according to the criteria proposed by Boeyens[34] and classified in terms of the six canonical conformations, namely, chair (C), boat (B), envelope (E), screw-boat (S), half-chair (H), and twist-boat (T). Thus, the conformation noted as $^1S_6$, for instance, corresponds to a screw boat puckered at atoms 1 and 6. For a molecule symmetric through ring plane reflection, $^1S_6$

(17) Sobolewski, A. L.; Domcke, W. *Eur. Phys. J. D* **2002**, *20*, 369–374.
(18) Chung, W. C.; Lan, Z. G.; Ohtsuki, Y.; Shimakura, N.; Domcke, W.; Fujimura, Y. *Phys. Chem. Chem. Phys.* **2007**, *9*, 2075–2084.
(19) Nix, M. G. D.; Devine, A. L.; Cronin, B.; Ashfold, M. N. R. *J. Chem. Phys.* **2007**, *126*, 124312–10.
(20) Serrano-Andrés, L.; Merchán, M.; Borin, A. C. *Chem. Eur. J.* **2006**, *12*, 6559–6571.
(21) Clark, L. B.; Peschel, G. G.; Tinoco, I. *J. Phys. Chem.* **1965**, *69*, 3615–3618.
(22) Li, L.; Lubman, D. M. *Anal. Chem.* **1987**, *59*, 2538–2541.
(23) Kim, N. J.; Jeong, G.; Kim, Y. S.; Sung, J.; Kim, S. K.; Park, Y. D. *J. Chem. Phys.* **2000**, *113*, 10051–10055.
(24) Kim, N. J.; Kang, H.; Jeong, G.; Kim, Y. S.; Lee, K. T.; Kim, S. K. *J. Phys. Chem. A* **2000**, *104*, 6552–6557.
(25) Nir, E.; Plutzer, C.; Kleinermanns, K.; de Vries, M. *Eur. Phys. J. D* **2002**, *20*, 317–329.
(26) Kim, N. J.; Kang, H.; Park, Y. D.; Kim, S. K. *Phys. Chem. Chem, Phys.* **2004**, *6*, 2802–2805.
(27) Broo, A.; Holmen, A. *J. Phys. Chem. A* **1997**, *101*, 3589–3600.
(28) Fleig, T.; Knecht, S.; Hättig, C. *J. Phys. Chem. A* **2007**, *111*, 5482–5491.
(29) Fulscher, M. P.; Serrano-Andres, L.; Roos, B. O. *J. Am. Chem. Soc.* **1997**, *119*, 6168–6176.
(30) Matsika, S. *J. Phys. Chem. A* **2005**, *109*, 7538–7545.
(31) Barbatti, M.; Lischka, H. *J. Phys. Chem. A* **2007**, *111*, 2852–2858.
(32) Ghigo, G.; Roos, B. O.; Malmqvist, P.-A. *Chem. Phys. Lett.* **2004**, *396*, 142–149.
(33) Cremer, D.; Pople, J. A. *J. Am. Chem. Soc.* **1975**, *97*, 1354–1358.
(34) Boeyens, J. C. A. *J. Chem. Crystallogr.* **1978**, *8*, 317–320.
(35) Fogarasi, G.; Zhou, X. F.; Taylor, P. W.; Pulay, P. *J. Am. Chem. Soc.* **1992**, *114*, 8191–8201.

and $^6S_1$ conformations are equivalent. For the five-membered rings, the conformations were related to the CP parameters according to the Cremer and Pople prescriptions.[33]

The mass-weighted distance (d_{MW}) between the geometry **r** and that of the ground-state minimum ($\mathbf{r}^0$) was computed according to the expression

$$d_{MW} = \left[\sum_{n=1}^{N_{at}} \sum_{i=1}^{3} m_n (r_{ni} - r_{ni}^0)^2\right]^{1/2} \quad (1)$$

where N_{at} is the number of atoms and m_n is the mass of the nth atom. To guarantee maximum overlap between the two geometries, before the distances were computed, the Cartesian coordinates of the MXSs were converted into internal coordinates and then converted back to Cartesian coordinates as described in ref 35 using the ground-state geometry as reference. Reaction paths were generated by linear interpolation of internal coordinates (LIIC). For the determination of cuts along the crossing seam, restricted search of the minimum on the crossing seam was performed for each point of the LIIC path defined between two conical intersections.

Mixed quantum-classical dynamics simulations were performed at the MR-CIS(6,4)/SA-4-CAS(12,10) level for 9*H*-Ade and at the SA-3-CAS(8,7)/6-31G* level for 6AP. In both cases 0.5 fs time steps were adopted. In the case of 9*H*-Ade, the 6-31G* basis set was used in the C and N atoms of the pyrimidine ring, while the 3-21G basis set was adopted for all other atoms. This choice of basis set will be referred as B_{mix}, and it is based on the fact that the main conical intersections in 9*H*-Ade correspond to deformations of the pyrimidine ring. The nuclei were treated classically, while the time-dependent Schrödinger equation was integrated for the electrons. The obtained time-dependent adiabatic populations were corrected for decoherence effects[36] ($\alpha = 0.1$ hartree) and used for computing the surface-hopping probabilities according to Tully's fewest switches approach.[37,38] The momentum was kept constant after frustrated hoppings and adjusted along the nonadiabatic coupling vector in the case of actual hoppings. In order to keep the calculations within reasonable computational costs, only hoppings to the state immediately below the current state were computed for 9*H*-Ade; thus, for example, the system in S_2 could hop to S_1 but not to S_0. The exception was the motion on the S_0 surface, for which the hopping probability to S_1 was also computed. The initial conditions were selected from a Wigner distribution for the quantum harmonic oscillator at the ground electronic and vibrational state. The same data were used for computing the absorption spectrum according to the Gaussian broadening method described in ref 39.

Sixty trajectories were computed for 9*H*-Ade starting at the L_a state (S_3 at the current level of calculation). Thirty trajectories were computed for 6AP starting at the S_2 state ($\pi\pi^*$). The motion of hydrogen atoms connected to C_4 and C_5 of 6AP were restricted by increasing their masses to 45 amu in order to simulate the mechanical restrictions of the imidazole group. This method, proposed by Warshel in the simulation of retinal,[40] has been used quite successfully in our previous simulations on the S_1 dynamics of 6AP.[31] The simulation time for the 9*H*-Ade trajectories was 600 fs. In the case of 6AP, the maximum time was 2 ps, but trajectories that hopped to the ground state and stayed there for more than 100 fs were terminated.

MXS searches and geometry optimizations were performed with the COLUMBUS program system.[41–43] CASPT2 calculations were performed with the MOLCAS 6.4 program.[44] The dynamics simulations were performed with the NEWTON-X package[39,45] using the analytical gradients[46–48] and nonadiabatic coupling vectors[49,50] provided by COLUMBUS. CP parameters were determined using the PLATON program.[51]

Table 1. Vertical Excitation Energies (eV) for 9*H*-Ade

		CASPT2[b]		
state	MR-CIS[a]	this work	Serrano-Andrés et al.[c]	exptl
S_0	0.00	0.00 (0.00)	0.00	
S_1	5.98 π^*	5.29 (4.96) nπ^*	4.96 nπ^*	
S_2	6.23 L_b	5.43 (5.03) L_b	5.16 L_b	
S_3	6.49 L_a	5.56 (5.17) L_a	5.35 L_a	4.98[d] (5.12[e])

[a] MR-CIS(6,4)/SA-4-CASSCF(12,10)/B_{mix} level used for the dynamics simulations; geometry optimized at the same level. [b] CASPT2/SA-5-CASSCF(16,12)/6-31G* method used for single -point calculations on geometries optimized at the MR-CIS(6,5)/SA-3-CAS(12,10)/6-31G* level. The values in parentheses were obtained using IPEA = 0.0. [c] CASPT2//CASSCF(16,13)/6-31G* method.[15] [d] Adenine vapor, maximum of the absorption band (249 nm).[21] [e] Vertical excitation estimated from the maximum of the absorption band (see text).

Results and Discussion

Vertical Excitation and Quality of the Potential Energy Surfaces. The lowest singlet vertical electronic transitions in 9*H*-Ade are to the bright L_a $\pi\pi^*$ state and to the L_b $\pi\pi^*$ and nπ^* states.[15,28] The computation of the precise ordering and energies of these states is an especially difficult task, due to the high sensitivity of the results to the theoretical method. For comparative data sets, see refs 8 and 11. In view of this situation, it was our goal to reproduce as closely as possible one of the most accurate results reported so far,[15] computed at the CASPT2//CASSCF(16,13)/6-31G* level. In Table 1, besides these benchmark and experimental[21] results, the current vertical excitation energies are presented as computed for the two main theoretical levels employed in this work: the MR-CIS approach used in the dynamics simulations and the CASPT2 approach used in the single-point calculations of the reaction paths. The results obtained at the CASPT2/SA-5-CASSCF(16,12)/6-31G* level are a few tenths of an electronvolt higher than the results

(36) Granucci, G.; Persico, M. *J. Chem. Phys.* **2007**, *126*, 134114–11.
(37) Tully, J. C. *J. Chem. Phys.* **1990**, *93*, 1061–1071.
(38) Hammes-Schiffer, S.; Tully, J. C. *J. Chem. Phys.* **1994**, *101*, 4657–4667.
(39) Barbatti, M.; Granucci, G.; Persico, M.; Ruckenbauer, M.; Vazdar, M.; Eckert-Maksic, M.; Lischka, H. *J. Photochem. Photobiol. A: Chem.* **2007**, *190*, 228.
(40) Warshel, A. *Nature* **1976**, *260*, 679–683.
(41) Lischka, H.; Shepard, R.; Brown, F. B.; Shavitt, I. *Int. J. Quantum Chem.* **1981**, *S.15*, 91–100.
(42) Lischka, H.; Shepard, R.; Pitzer, R. M.; Shavitt, I.; Dallos, M.; Müller, T.; Szalay, P. G.; Seth, M.; Kedziora, G. S.; Yabushita, S.; Zhang, Z. Y. *Phys. Chem. Chem. Phys.* **2001**, *3*, 664–673.
(43) Lischka, H.; Shepard, R.; Shavitt, I.; Pitzer, R. M.; Dallos, M.; Mueller, T.; Szalay, P. G.; Brown, F. B.; Ahlrichs, R.; Boehm, H. J.; Chang, A.; Comeau, D. C.; Gdanitz, R.; Dachsel, H.; Ehrhardt, C.; Ernzerhof, M.; Hoechtl, P.; Irle, S.; Kedziora, G.; Kovar, T.; Parasuk, V.; Pepper, M. J. M.; Scharf, P.; Schiffer, H.; Schindler, M.; Schueler, M.; Seth, M.; Stahlberg, E. A.; Zhao, J.-G.; Yabushita, S.; Zhang, Z.; Barbatti, M.; Matsika, S.; Schuurmann, M.; Yarkony, D. R.; Brozell, S. R.; Beck, E. V.; Blaudeau, J.-P. COLUMBUS, an ab Initio Electronic Structure Program, release 5.9.1; 2006, www.univie.ac.at/columbus.
(44) Karlström, G.; Lindh, R.; Malmqvist, P. A.; Roos, B. O.; Ryde, U.; Veryazov, V.; Widmark, P. O.; Cossi, M.; Schimmelpfennig, B.; Neogrady, P.; Seijo, L. *Comput. Mater. Sci.* **2003**, *28*, 222–239.
(45) Barbatti, M.; Granucci, G.; Lischka, H.; Ruckenbauer, M.; Persico, M. NEWTON-X: a Package for Newtonian Dynamics Close to the Crossing Seam, version 0.14b; 2007, www.univie.ac.at/newtonx.
(46) Shepard, R.; Lischka, H.; Szalay, P. G.; Kovar, T.; Ernzerhof, M. *J. Chem. Phys.* **1992**, *96*, 2085–2098.
(47) Shepard, R. In *Modern Electronic Structure Theory*; Yarkony, D. R., Ed.; World Scientific: Singapore, 1995; Vol. 1, p 345.
(48) Lischka, H.; Dallos, M.; Shepard, R. *Mol. Phys.* **2002**, *100*, 1647–1658.
(49) Dallos, M.; Lischka, H.; Shepard, R.; Yarkony, D. R.; Szalay, P. G. *J. Chem. Phys.* **2004**, *120*, 7330–7339.
(50) Lischka, H.; Dallos, M.; Szalay, P. G.; Yarkony, D. R.; Shepard, R. *J. Chem. Phys.* **2004**, *120*, 7322–7329.
(51) Spek, A. L. *J. Appl. Crystallogr.* **2003**, *36*, 7–13.

of ref 15. The reason for that is the usage of the IPEA shift,[32] as mentioned in the Computational Details. If the conventional noncorrected perturbative Hamiltonian is used (Table 1, in parentheses), our CASPT2 results are in excellent agreement with the benchmark results. As reported in several cases, the maximum of the absorption spectrum is found at lower energies than the actual vertical excitation energy.[39,52–54] According to the results of simulations of the UV absorption spectrum shown in Figure SI1 of the Supporting Information, this difference is computed as 0.14 eV for the L_a band. Therefore, the "experimental" vertical excitation energy is estimated to be located at 5.12 eV. On the basis of this result, the data with the IPEA shift seem to overestimate the vertical excitation energy by 0.44 eV.

The results obtained at the MR-CIS level are about 0.8−0.9 eV higher than the CASPT2 results, which represents an acceptable compromise given the difficulties for combining quality and computational efficiency demanded by the extremely expensive on-the-fly dynamics simulations where a full quantum chemical calculation has to be performed at every time step. The MR-CIS results show the same order of states and similar S_1/S_2 and S_2/S_3 energy gaps in comparison to the CASPT2 calculations. In addition to that, all conical intersections and reaction paths computed at the CASPT2 level that will be discussed in the next section can also be adequately described at the MR-CIS level (see Figures SI2 and SI3 in the Supporting Information). The vertical shift to higher energies observed in the vertical excitation computed at the MR-CIS level also occurs to a large extent along the reaction paths, which means that the kinetic energy during the dynamics does not become artificially high. Since this compensation is not perfect, the MR-CIS calculations present overall a more sloped surface, which should speed up the dynamics and produce slightly shorter lifetimes than would be obtained if the dynamics were performed at a more extended computational level.

S_1/S_0 Conical Intersections in 9*H*-Adenine. In our previous investigations on 6AP, chosen as a model system for adenine,[31,55–57] five different minima on the crossing seam (MXS) have been found, which were formed by different kinds of ring puckering at the envelope conformations ^2E and E_4, at the screw-boat conformations $^1S_6$ and $^4S_3$, and at the boat conformation $B_{3,6}$. For their characterization in terms of the CP parameters, see Figure 2. Because of the similarities between 6AP and 9*H*-Ade, we expected that a similar structure of the crossing seam exists for the nucleobase as well. Indeed, the search performed for the MXS of 9*H*-Ade has resulted in similar puckered structures, which are characterized in Figure 2 and Table 2. Their structures are shown in Figure 3. The Cartesian coordinates are given in the Supporting Information.

The ^2E MXS corresponds to the global minimum on the crossing seam (see Table 2) and has already been reported previously.[9–13,15] The second lowest-energy MXS is the $^1S_6$ structure, whose main feature is the out-of-plane distortion of the amino group. It was also described previously.[9,10,13,15] The $^4S_3$, $B_{3,6}$, $^2H_3$, and E_3 structures correspond, however, to new conical intersections and have not been reported before. The E_3 and $^2H_3$ conical intersections are not true minima on the crossing seam. They have been obtained by restricting some torsional angles during the optimization procedure in order to avoid the collapse into the ^2E MXS. The restricted optimization of these conical intersections was performed in order to explore the branch of crossing seam starting at the ^2E MXS.

In addition to the conical intersections formed by the puckering of the pyrimidine ring, there exist other intersections formed either by puckering of the imidazole ring or by bond breaking. On the basis of the analogous conical intersection found in the pyrrole,[58] we have characterized a new MXS formed by the puckering of the C_8 atom (envelope E_8 conformation). Concerning the bond-breaking regions of the crossing seam, conical intersections characterized by the C_8-N_9, N_9-H, and $N_{amino}-H$ bond dissociation have been characterized in detail by Sobolewski et al.[59] and Perun et al.[14,17]

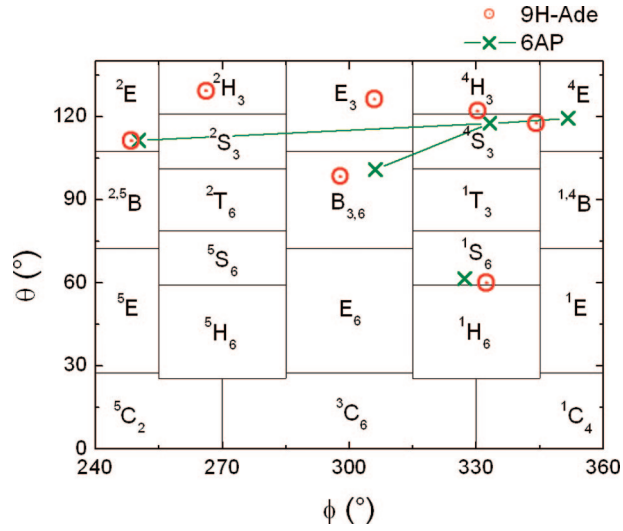

Figure 2. MXSs in 9*H*-Ade (circles) and 6AP (crosses) in the space of the CP parameters $\theta-\phi$. The different domains in this plane correspond to the conformer classification proposed by Boeyens.[34]

Table 2. Characterization of the Puckered Conical Intersections in 9*H*-Adenine[a]

					ΔE (eV)	
conform.	Q (Å)	θ (deg)	φ (deg)	d_{MW} (amu$^{1/2}$ Å)	MR-CIS[b]	CASPT2[c]
^2E	0.54	111	248	3.43	4.61	3.98
$^1S_6$	0.46	120	152	6.01	5.29	4.33
E_3	0.53	126	306	3.39	5.54	4.94
$B_{3,6}$	0.72	82	118	5.37	6.17	5.14
E_8	0.48		319	3.41	6.16	5.19
$^4S_3$	0.64	63	164	5.43	6.25	5.43
$^4H_3$	0.36	122	330	5.52	5.77	5.52
$^2H_3$	0.63	129	266	3.54	5.65	5.54

[a] Geometric parameters obtained at the MR-CIS(6,5)/SA-3-CAS-(12,10)/6-31G* level. [b] MR-CIS(6,4)/SA-4-CASSCF(12,10)/B_{mix} method used also for the dynamics simulations on geometries optimized at the same level. [c] CASPT2/SA-5-CASSCF(16,12)/6-31G* method used for single-point calculations on geometries optimized at the MR-CIS(6,5)/SA-3-CAS(12,10)/6-31G* level.

(52) Davidson, E. R.; Jarzecki, A. A. *Chem. Phys. Lett.* **1998**, *285*, 155–159.
(53) Müller, T.; Dallos, M.; Lischka, H. *J. Chem. Phys.* **1999**, *110*, 7176–7184.
(54) Bomble, Y. J.; Sattelmeyer, K. W.; Stanton, J. F.; Gauss, J. *J. Chem. Phys.* **2004**, *121*, 5236–5240.
(55) Barbatti, M.; Ruckenbauer, M.; Szymczak, J. J.; Aquino, A. J. A.; Lischka, H. *Phys. Chem. Chem. Phys.* **2008**, *10*, 482.
(56) Barbatti, M.; Sellner, B.; Aquino, A. J. A.; Lischka, H. In *Radiation Induced Molecular Phenomena in Nucleic Acid*; Shukla, M. K., Leszczynski, J., Eds.; Springer: Dordrecht, The Netherlands, 2008.
(57) Zechmann, G.; Barbatti, M. *Int. J. Quantum Chem.* **2008**, *108*, 1266.
(58) Barbatti, M.; Vazdar, M.; Aquino, A. J. A.; Eckert-Maksic, M.; Lischka, H. *J. Chem. Phys.* **2006**, *125*, 164323.
(59) Sobolewski, A. L.; Domcke, W.; Dedonder-Lardeux, C.; Jouvet, C. *Phys. Chem. Chem. Phys.* **2002**, *4*, 1093–1100.

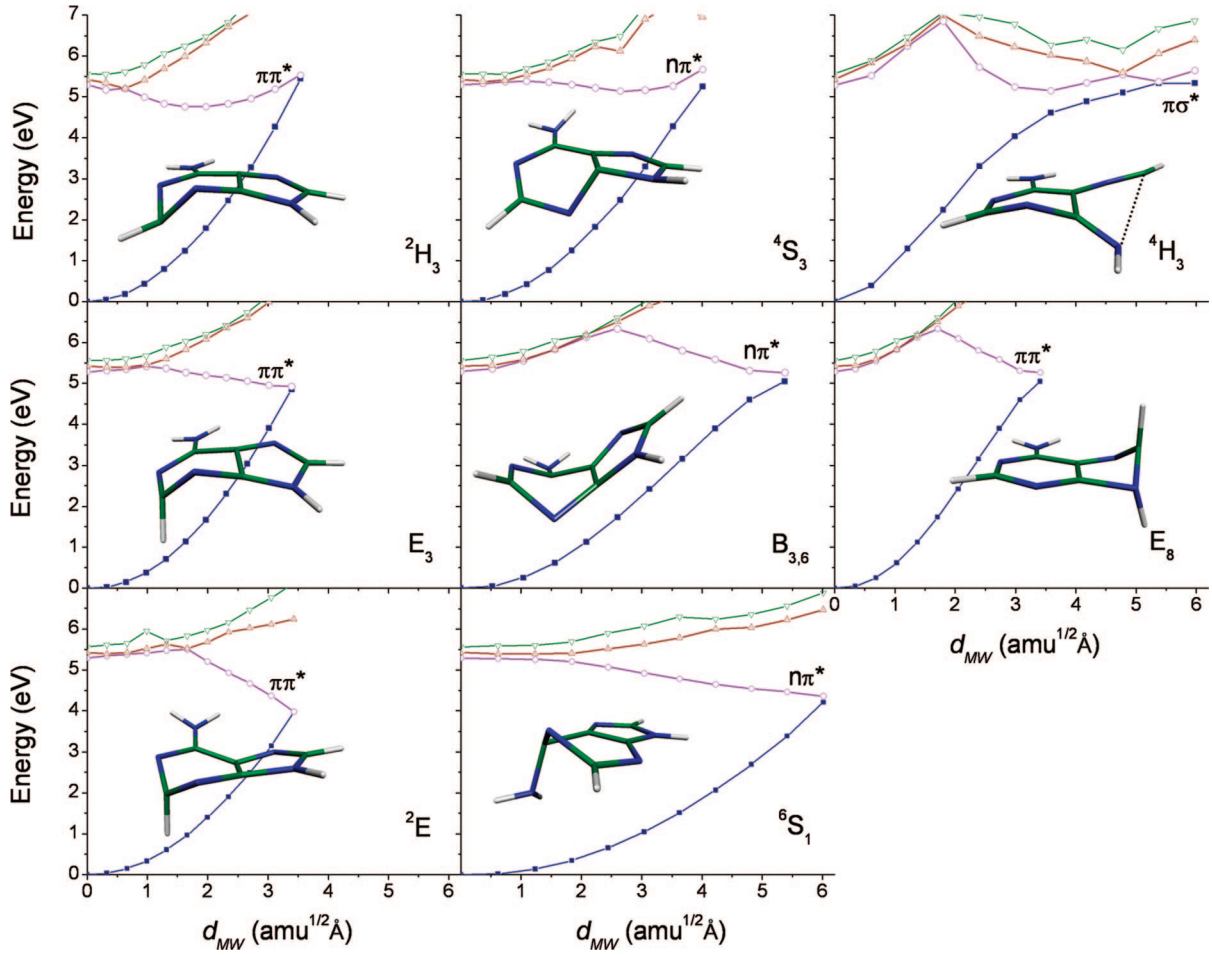

Figure 3. Paths connecting the ground-state minimum geometry to the puckered MXSs. The MXS geometry is shown in each case.

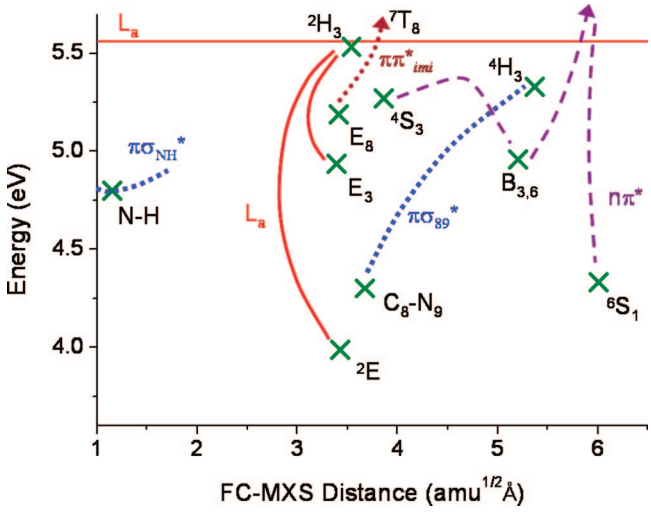

Figure 4. Energy of the MXSs of 9*H*-Ade as function of the mass-weighted distance between the FC region and the MXS. The horizontal line indicates the vertical excitation energy (L_a state). The lines connecting the MXSs schematically indicate the crossing seam branches.

Several of these conical intersections possess energies below the vertical excitation energy of the L_a $\pi\pi^*$ state, as is shown in Figure 4. In this figure, the energies are given relative to the minimum of the ground state as a function of the distance in mass-weighted (d_{MW}) coordinates between the ground-state minimum geometry and the respective MXS geometry (see Computational Details). Sketches characterizing the branches of the intersection seam connecting different MXSs are given in Figure 4 as well.

As have been revealed by dynamics of 9*H*-Ade and 6AP (see below), these conical intersections are interconnected by branches of the crossing seam. In the first branch, the ^2E MXS is connected to the $^2H_3$ and E_3 conical intersections. In this branch, the S_1 state has the same $\pi\pi^*$ character as the bright L_a state. In the second branch of the crossing seam, the E_8 MXS characterized by distortions in the imidazole group is connected to conical intersections of the twist-boat $^7T_8$ conformation (see Figure SI4 in the Supporting Information). In another branch of crossing seam, the planar C_8-N_9 open-ring MXS is connected to open-ring conical intersections showing out-of-plane deformations such as the $^4H_3$ MXS (see Figure SI5 in the Supporting Information). The excited state in this branch has $\pi\sigma_{89}$* character, with the σ_{89}* orbital located in the C_8-N_9 broken bond. The $^4S_3$ and the $B_{3,6}$ MXSs are connected by another branch of the crossing seam, whose S_1 state has $n\pi^*$ character, as also shown by the 6AP dynamics (see below). This branch extends to the $^1S_6$ MXS, which has $n\pi^*$ character (see Figure SI6 in the Supporting Information). Finally, other branches of the crossing seam exist for the N_9H and $N_{amino}H$ stretchings. The S_1 state has $\pi\sigma_{NH}$* character in these cases.

Figure 3 shows the paths connecting the Franck−Condon region (ground-state minimum) to each of the puckered MXSs. The paths were obtained by linear interpolation of internal coordinates (LIIC) and are given as a function of the mass-

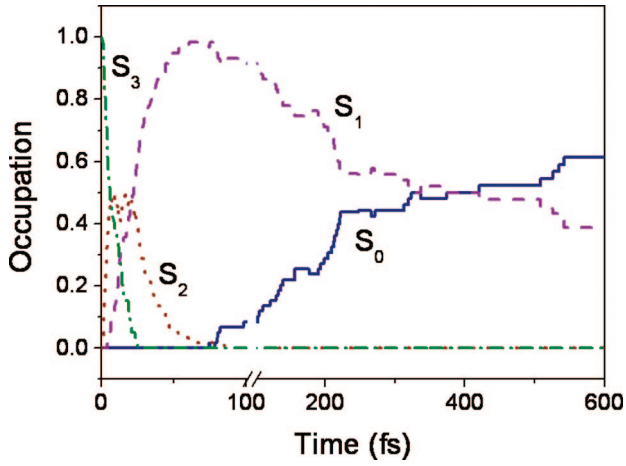

Figure 5. Fraction of trajectories (occupation) in each state as a function of time.

weighted distance to the Franck−Condon region. The energies were calculated at the CASPT2/CASSCF(16,12)/6-31G* level. The data displayed in Figure 4 and Table 2 show that the ^{2}E MXS is the conical intersection with the lowest energy. The $\pi\pi^*$ diabatic connection along the path to the ^{2}E MXS is practically barrierless at the CASPT2/CASSCF(16,12)/6-31G* level, showing a very small barrier of 0.04 eV, which should disappear upon relaxation (see Figure SI3 in the Supporting Information). Note that the hump in the S_3 state at 1 amu$^{1/2}$ Å does not belong to the aforementioned $\pi\pi^*$ diabatic connection. Near the MXS, the S_1 state has the same electronic configuration as the bright L_a state and is one of the MXSs which requires the smallest deformation with respect to the FC region in terms of the mass-weighted distance d_{MW}. Both factors contribute to making it the conical intersection to be most likely accessed in the deactivation process of 9*H*-Ade, as is confirmed by the dynamics simulations discussed below. The $^1S_6$ MXS, on the other hand, is also situated in the low-energy region. Much larger deformations are necessary in order to reach it from the FC region. The C_8−C_9 planar ring opening MXS (see reaction path in ref 14) combines low-energy and relatively short distances to the FC region. It depends, however, on the change of the electronic configuration from $\pi\pi^*$ to $\pi\sigma^*$, which involves a rather high energy barrier,[14] thereby decreasing its efficiency. The NH stretching MXSs, although lying very close to the FC region, appear at relatively high energies and depend also on a transformation of the electronic configuration.[13,14]

Dynamics Simulations and the Two-Step Relaxation Process. The dynamics simulations show that, starting in the L_a $\pi\pi^*$ (S_3) state, the 9*H*-Ade relaxation proceeds extremely quickly. The S_3 state is completely depopulated in less than 25 fs (see Figure 5), while the population of the S_2 state increases to 50% at around 15 fs. The $S_2 \rightarrow S_1$ transfer occurs simultaneously with the $S_3 \rightarrow S_2$ transfer, and practically all trajectories (98.3%) are already in S_1 after 60 fs. After 75 fs, the $S_1 \rightarrow S_0$ transfer starts and the S_1 occupation decays exponentially.

This situation implies a two-component decay, one ultrashort step corresponding to the $S_3 \rightarrow S_2 \rightarrow S_1$ relaxation process and another longer step corresponding to the $S_1 \rightarrow S_0$ transfer. By fitting the S_1 occupation curve given in Figure 5 with the unimolecular decay model

$$f(t) = \frac{\tau_2}{\tau_1 - \tau_2}\left[\exp\left(\frac{-t}{\tau_1}\right) - \exp\left(\frac{-t}{\tau_2}\right)\right] \qquad (2)$$

Table 3. Survey of Lifetime Results for 9*H*-Ade in the Gas Phase

	λ_{pump} (nm)	τ_1 (fs)	τ_2 (ps)	τ_3 (fs)
current data	complete band	22	0.538	
exptl ref 1, 2	267		1.00	
exptl ref 7	267		0.97	
exptl ref 7	276		1.8	
exptl ref 4	267	100	1.10	
exptl ref 5, 6	267	40	1.2	
exptl ref 3	277		>2	$\sim 10^6$
exptl ref 3	267	<50	0.75	$\sim 10^6$
exptl ref 3	250	<50	0.75	$\sim 10^6$

the values $\tau_1 = 22$ fs and $\tau_2 = 538$ fs are obtained. The current dynamics simulations, therefore, corroborate the interpretation that attributes the relaxation into S_1 to the short-time-step component and that into S_0 to the long step. The good exponential fitting of the S_1 population indicates that the long time step corresponds to a microcanonical equilibration of the population in the S_1 state, with a subsequent decay to S_0 proportional to this population. We could not find any evidence of direct deactivation before this equilibration, as proposed by Serrano-Andrés et al.,[15] although the possibility of its occurrence cannot be discarded for a minor fraction of trajectories decaying before 100 fs. It will be shown in the next section, however, that the claim by Serrano-Andrés et al. concerning the activation of the ^{2}E conical intersection in the short time scale is still valid.

The $S_3 \rightarrow S_2 \rightarrow S_1$ relaxation process occurs in a region where several electronic states are located closely together, as can already be seen from the vertical excitation energies (Table 1). Although the current simulations are prepared to deal only with sequences of two-state transitions, the ultrafast deactivation within 22 fs corroborates the hypothesis raised by Matsika[30] that three-state conical intersections should play a role in this initial step. Consider, for instance, the $S_3 \rightarrow S_2$ transition. It occurs after 9 fs (mean value) with average energy gaps $\Delta E_{32} = 0.2 \pm 0.1$ eV and $\Delta E_{21} = 0.4 \pm 0.2$ eV (see Figure SI7 in the Supporting Information). These gaps are small enough to deserve a three-state treatment.

The computed decay times of 22 and 538 fs, respectively, are in very good agreement with the <50/750 fs measured by Ullrich et al.[3] (see Table 3). These experimental values are, however, shorter than those derived from other measurements, which predict lifetimes of about 1 ps for the 267 nm excitation. The main reason for this shorter theoretical lifetime is the fact that the lifetime of adenine shows a strong dependence on the photoexcitation energy, which decreases from about 1.8 ps at 276 nm to about 0.97 ps at 267 nm according to Chin et al.[7] In the present simulations, the complete absorption band centered at the vertical excitation energy was used to select the initial conditions for the dynamics (see Figure SI1 in the Supporting Information). This higher average initial energy should have the effect of reducing the lifetime. In fact, the present results would be more properly comparable with lifetimes measured with a pump energy at around 4.98 eV (249 nm), an energy which corresponds to the experimental band maximum in the gas phase (Table 1).[21] Another reason for the discrepancies was already anticipated and can be attributed to the shape of the MR-CIS surfaces.

Role of Different Conical Intersections. As has been discussed above, a large number of qualitatively different S_0/S_1 conical intersections exist for 9*H*-Ade formed either by ring puckering or by bond breaking geometric deformations. These intersections are connected by extended branches of the crossing seam. The

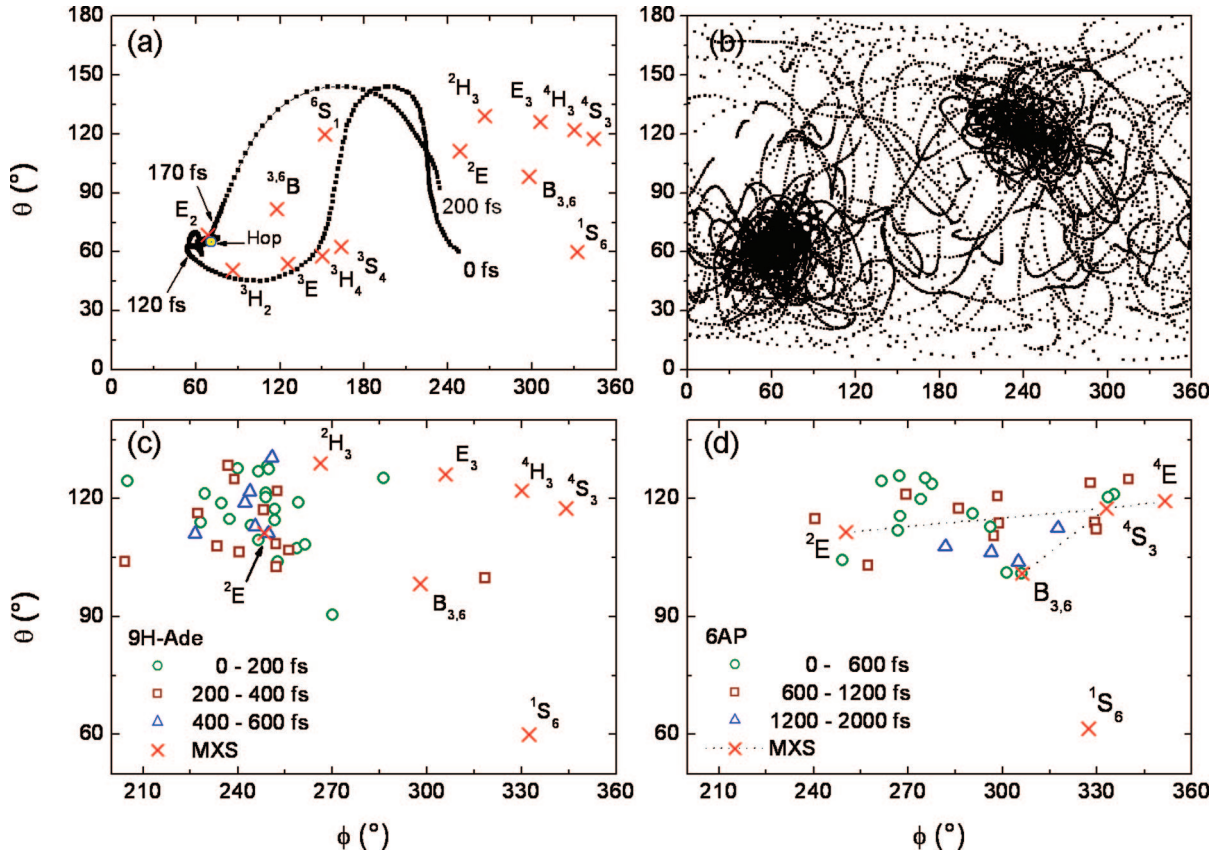

Figure 6. Puckered conformations in the 9*H*-Ade dynamics: (a) one single trajectory; (b) all trajectories; (c) conformations at the $S_1 \rightarrow S_0$ hopping time; (d) puckered conformations at the hopping time for 6AP. The crosses indicate the location of the MXSs.

analysis of the features of these conical intersections and of the reaction paths connecting them to the FC region indicated that the ^{2}E conical intersection should be the most important one for the nonadiabatic deactivation. The dynamics simulations confirm this analysis showing that during the first 600 fs the out-of-plane distortions of the pyrimidine ring of 9*H*-Ade in the S_1 state are mainly concentrated in the region between the ^{2}E and $^2H_3$ conformations, where almost all hopping events take place (see Figure 6c), independently of the initial excitation energy and of the hopping time. This means that for the broad range of excitations energies used in the present simulations 9*H*-Ade returns to the ground-state mostly in the $\pi\pi^*/S_0$ region of the crossing seam. As predicted by Serrano-Andrés et al.,[15] the ^{2}E conical intersection can be activated as soon as 100 fs.

One single trajectory followed a completely different reaction path and deactivated near the C_8-N_9 bond breaking conical intersection after 80 fs. The initial energy of this particular trajectory was 0.6 eV above the vertical excitation energy into the L_a state: therefore, in the extreme of the blue tail of the absorption band. This event confirms that high-energy photoexcitation can activate $\pi\sigma^*/S_0$ deactivation paths, as has been discussed by Perun et al.[14] No conical intersections showing N−H stretching were observed. This can be partially explained by the high-energy threshold for the activation of these reaction paths to the conical intersections, corresponding to wavelengths below 233 nm according to the experiments of Nix et al.[19] A threshold of 267 nm, as proposed by Satzger et al.,[6] is too low to be compatible with the present results. Although the theoretical level employed in the current simulations should be improved in order to treat more adequately this kind of conical intersection, we want to note in addition that the occurrence of the deactivation at the $\pi\sigma^*/S_0$ conical intersection after low-energy excitation is difficult to rationalize in terms of the lack of radiationless decay in 2-aminopurine,[15] where the same ultrafast deactivation via N−H dissociation could occur.

In order to investigate which kinds of conical intersections are involved in the deactivation on the long time scale (until 2 ps), we have performed mixed quantum−classical dynamics for 6AP starting in the S_2 state and imposing mechanical restrictions (see Computational Details). This set of trajectories was designed especially to model adenine dynamics starting at the L_a state. If we collect the 6AP structures at the S_1/S_0 hopping time corresponding to an energy gap of less than 0.5 eV and plot the corresponding CP parameters in the $\theta-\varphi$ space, we obtain the distribution shown in Figure 6d. The figure shows that the hoppings are concentrated along the region between the ^{4}E and ^{2}E conformations. This implies that the crossing seam connects all these MXSs, as indicated by the dashed lines in Figure 6d.

The distribution of S_0/S_1 hoppings shows that at later times they are displaced toward the E_3 and ^{4}E conformations (see also Figure 2). It is remarkable, however, that in these results as well as in those obtained from previously performed dynamics simulations for 6AP,[31,55,56] which correspond to a total of 120 trajectories, the $^1S_6$ MXS conformation corresponding to an out-of-plane motion of the NH_2 group was never accessed for deactivation. On the basis of the dynamics results we cannot even say whether or not this conical intersection is connected to the main branch of crossing seam, although the restricted optimization on the crossing seam have shown that it is. This finding is a strong indication that the deactivation of 9*H*-Ade proceeds without involving the $^1S_6$ conical intersection seam.

There is no energetic reason for the absence of $^1S_6$ conical intersections during the 9*H*-Ade and 6AP dynamics. As we have discussed above, this MXS lies in a low-energy region and the barriers along the reaction path are not larger than 0.08 eV.[15] The $^1S_6$ conical intersection, however, requires a strong geometrical deformation, as the distances in Table 2 show. Therefore, the trajectories converge and remain trapped near ^{2}E conformations (see Trapping Effect) long before they have the possibility to reach the $^1S_6$ conformations with a relatively high degree of puckering.

Trapping Effect. The efficiency of a conical intersection is strongly connected to the shape of the energy surfaces nearby beyond the linear region. If the surface is such that the molecule stays trapped there for some time, the molecule may have time to find the appropriate coordinate values that tune the conical intersection. Such an effect has been found by us, for example, in substituted ethylenes where the torsional mode and the central bond length required appropriate adjustment in order to reach the conical intersection.[60–62] If the shape of the energy surface is not favorable, the molecule can indeed quickly approach the neighborhood of the seam of conical intersections but move on to other regions of the configuration space before having time for deactivation.

This "trapping effect" can be nicely observed in Figure 6a. There, the Cremer−Pople parameters θ and ϕ are given along a single trajectory for 9*H*-Ade starting in the S_3 state. In this particular trajectory, 9*H*-Ade moves along a sequence of conformations with conical intersections ($^3S_4$, $^3H_4$, ...) without hopping. Even though the CP coordinates θ and ϕ assume the appropriate values for approaching the conical intersections, at least some of the other coordinates do not have the "right" values. When 9*H*-Ade is in the half-chair $^3H_2$ conformation, for example, the degree of puckering (as shown in the movie provided in the Supporting Information) is relatively small with a value Q of ~0.2 Å. At these structures the energy gap shows values of about 2−3 eV, which are not small enough for efficient nonadiabatic coupling and concomitant surface hopping. Q values of ~0.5 Å would be needed for that purpose. If the shape of the S_1 surface were such that 9*H*-Ade remained trapped near the $^3H_2$ conformation, it could eventually tune the right Q value for a closer approach to the conical intersection and decay there. What occurs, however, is that 9*H*-Ade does not remain long enough in the $^3H_2$ conformation and changes to the ^{2}E envelope conformation. As can be seen in Figure 6a, 9*H*-Ade is trapped in this last conformation and moves there around until the hopping to the ground state takes place.

Elsewhere we have discussed the case of 2-pyridone,[62] for which the surface shape makes the trajectories spread over the complete conformation space without being trapped in any particular region. As a result, the molecule does not find the available conical intersections and becomes a fluorescent species. With 9*H*-Ade it seems that exactly the opposite happens. The complete set of trajectories converges to the ^{2}E region (Figure 6b) and stays there until finding the conical intersection.

The trajectory depicted in Figure 6a remained in the $\pi\pi^*$ state until the hopping time. The $n\pi^*$ state was never accessed. This exclusive population of the $\pi\pi^*$ state was observed in most of the investigated trajectories and corroborates the analysis of ref 15, which predicted that the deactivation of 9*H*-Ade through the ^{2}E MXS would occur by means of a diabatic $\pi\pi^*$ reaction path.

Conclusions and Outlook

On the basis of the conical intersections optimized at the CASSCF and MR-CIS levels, on CASPT2 reaction paths, and on the MR-CIS mixed quantum−classical dynamics simulations for 9*H*-adenine and 6-aminopyrimidine, we can draw the following conclusions concerning the ultrafast deactivation of 9*H*-Ade.

(1) A large variety of qualitatively different S_0/S_1 conical intersections exists for 9*H*-Ade. New intersection structures have been found beyond those known in the literature. The crossing seam extends into several branches, showing different kinds of puckering at the pyrimidine and imidazole rings and also bond-breaking features.

(2) The population transfer between states proceeds within two major steps and can be well-described by an exponential behavior. The first step is characterized by an ultrashort $S_3 \rightarrow S_2 \rightarrow S_1$ relaxation and takes about 22 fs. The second step corresponds to the $S_1 \rightarrow S_0$ relaxation and requires about 0.5 ps. The differences from the experimental results (<100/1000 fs) can be explained by differences in the excitation energies used in the experiment simulations (red tail of the absorption band) as compared to our simulations (band maximum) and by an overshooting in excitation energies by the MR-CIS method. The current dynamics simulations, therefore, corroborate the interpretation that attributes the relaxation into S_1 to the short-time-step component and into S_0 to the long step. We could not find any evidence of direct deactivation before this equilibration, as proposed by Serrano-Andrés et al.[15]

(3) After the relaxation into S_1, adenine remains trapped almost exclusively in the neighborhood of the envelope ^{2}E conformation until deactivation. Effectively, only conical intersections showing conformations close to the envelope ^{2}E ($\pi\pi^*/S_0$) intersection occur for the $S_1 \rightarrow S_0$ nonradiative decay. Following an exponential decay pattern, the ^{2}E conical intersections are accessed as early as 100 fs.

(4) Conical intersections with the $^1S_6$ (NH_2 out-of-plane) conformation were never observed in the dynamics simulations for 9*H*-Ade and 6AP and, therefore, cannot be used to explain the long time step as has been done in refs 9, 10, 14, and 15. Since there is no energetic reason for blocking the occurrence of this kind of conical intersection, the main reason for its absence are probably the large geometrical distortions required to reach it and the facile availability of the conical intersections around the ^{2}E conformation.

(5) One single trajectory excited from the blue tail of the absorption band decayed near the C_8-N_9 bond-breaking conical intersection ($\pi\sigma^*/S_0$). Conical intersections showing N−H bond breaking were not observed at all. This is consistent with the experiments showing that the they occur at wavelengths below 233 nm[19] but not with experiments putting this threshold at 267 nm.[6] We cannot discard, however, the possibility that the current theoretical level may not be adequate for the description of this kind of process. This point will be addressed in further work.

Our simulations clearly show the importance of dynamics simulations for the assignment of photochemical reaction mechanisms to specific lifetimes. It is virtually impossible to deduce from the extended static information on the energy

(60) Barbatti, M.; Aquino, A. J. A.; Lischka, H. *Mol. Phys.* **2006**, *104*, 1053–1060.
(61) Zechmann, G.; Barbatti, M.; Lischka, H.; Pittner, J.; Bonačić-Koutecký, V. *Chem. Phys. Lett.* **2006**, *418*, 377–382.
(62) Barbatti, M.; Aquino, A. J. A.; Lischka, H. *Chem. Phys.* **2008**, in press (doi: 10.1016/j.chemphys.2008.02.007).

surfaces, which is available in form of reaction paths, conical intersections, and partial coverage of the crossing seam, the adequate dynamic behavior in case of 9*H*-adenine. The reason for this finding is that it is very difficult to predict a priori the amount of time which the molecular system will spend in the neighborhood of different, energetically accessible types of conical intersections, since the various puckering coordinates are strongly coupled. The on-the-fly nonadiabatic dynamics is an expensive but very promising tool for elucidating detailed features of ultrafast photochemical processes.

Acknowledgment. This work was supported by the Austrian Science Fund within the framework of the Special Research Program F16 (Advanced Light Sources) and Project P18411-N19. We are grateful for technical support and computer time at the Linux PC cluster Schrödinger III of the computer center of the University of Vienna.

Supporting Information Available: A simulated absorption spectrum (Figure SI1), graphical comparison between CASPT2 and MR-CIS methods (Figures SI2 and SI3), cuts along the crossing seam (Figures SI4−SI7), energy gap distributions (Figure SI8), the complete ref 43, Cartesian coordinates for stationary structures and conical intersections, and a movie showing one 9*H*-Ade trajectory. This material is available free of charge via the Internet at http://pubs.acs.org.

JA800589P